Modeling color with and without an observer

A. Kimball Romney

Institute of Mathematical Behavioral Sciences, University of California, Irvine, CA 92697-5100

The application of a recently published model for color coding reveals that the locations in perceptual color space of the reflectance spectra of the Munsell color chips, after being projected through an orthonormal projection space derived from the three cone sensitivity curves of a normal human observer, are almost identical to the location in a physical color space obtained without an observer. Additional evidence confirming the model is presented, and sample applications demonstrate that the model provides functional explanations for previously unaccounted-for phenomena.

OCIS codes: 330.0330, 330.1690, 330.1720.

1. INTRODUCTION

Romney and Chiao [1] present a model for estimating how humans perceive the color of Munsell [2] color chips. Estimates are calculated for four variants of human observers; trichromats (with three photoreceptor cones), protanopes (lacking a long wavelength-sensitive cone), deuteranopes (lacking a medium wavelength sensitive cone), and tritanopes (lacking a short wavelength sensitive cone). The model assumes cone receptors as defined by Stockman and Sharpe [3], although it can also make estimates for any observer with known sensitivity curves that differ in location or variance from the Stockman and Sharpe specifications. Romney and Chiao apply their model to the appearance of the color of single color chips observed on a neutral background in normal daylight. Under these constraints we can model the color appearance of the 1269 Munsell chips from their reflectance spectra. When the color appearance coordinates generated from the model are compared with the internationally recognized CIE L*a*b* [4] color appearance coordinates, the results are remarkably similar as shown in Fig. 1, adapted from Romney and Chiao's Fig. 2 [1].

Basically the model calculates an orthonormal projection matrix from the cone sensitivity curves. The cube-rooted reflectance spectra are then multiplied by the

projection matrix, converting each reflectance spectrum into a linear transform of the cone sensitivity curves. This means that the visible portion of any spectrum (exemplified by the 1269 Munsell chips in Fig. 1) is represented by some weighted combination of the cone receptors. The strong claim of the model is that it provides a precise estimate of the way any specified observer perceives the relative distances among the Munsell color chips represented in a three-dimensional Euclidean space. The model uses singular value decomposition to calculate two sets of three-dimensional Euclidean coordinates; the first specifies the locations of the 1,269 Munsell chips and the second specifies the locations of each of the 301 wavelengths of spectral light.

[Place Fig. 1 about here]

In Fig. 1 the colored filled circles represent the location obtained for the Munsell chips while the line formed by the black dots represents the wavelength location of the spectral lights from 400 nm to 700 nm and is here called the *spectral color boundary*. In the earlier paper it was called *wavelength envelope*. This boundary represents the chromatic sensitivity of the normal human observer. In Fig. 1 the relative size of the chip locations and the spectral color boundary is arbitrary but the angular relationship between them is valid, which means that the predicted hue of the spectral monochromatic light at each wavelength is correctly represented by the spectral color boundary compared to the color chip locations. Note that there are no spectral lights in the purple region and this fact is correctly represented with zero sensitivity of the visual system in this region.

The model [1] describes how the shape of the spectral color boundary in Fig. 1 provides a functional explanation for why in additive mixtures of lights the color of red, green, and blue are uniquely determined by human observer chromatic sensitivity characteristics that define the boundary. An equally satisfactory functional explanation for the subtractive color locations is provided by observing that they are the complements of the additive colors, namely, cyan, magenta, and yellow. The locations of these colors are shown in Fig. 1 identified by their initial letter. Computational procedures and a detailed description of the model may be found in the original article [1]. In the following section the relationship between the model and earlier research is investigated.

2. RELATING THE MODEL TO EARLIER RESEARCH

Perhaps the most significant implication of the model is the rediscovery of the proper shape of the spectral color boundary as shown in Fig. 1. Romney and Chiao report that the sensitivity of the human visual system to monochromatic spectral lights is proportional to how far the spectral color boundary curve is from the origin. In Fig. 1 the second and third coordinates are plotted while Fig. 3A shows all three coordinates plotted against wavelength. In order to understand the model it is critical to note that after the cube-rooted data matrix of the 1,269 by 301 reflectance spectra has been multiplied by the projection matrix, each resulting spectrum can be reconstructed exactly by some weighted combination of the curves shown in Fig. 3A. These curves are a linear transformation of Stockman and Sharpe [3] cone sensitivity curves which in turn are a linear transformation of the Stiles and Burch [5,4] color matching functions. Since the curves in Fig. 3A are entirely a function of the human color matching functions and the cone sensitivities, we interpret them as representing the sensitivities of the human visual system.

To obtain a representation of the sensitivity of the visual system on the wavelength scale we compute the Euclidean distance of the three curves from the origin shown in Fig. 3A and plot the results in Fig. 2. Below, we demonstrate that this sensitivity curve and its representation as a spectral color boundary provides greater explanatory power than the spectral locus in the CIE chromaticity diagram [4]. We claim no originality for Figs. 1 and 2. For example, despite earlier forerunners, three publications by Cohen [6] and his coauthors [7,8] deserve priority for most of the concepts embodied in the figures. The critical step they missed is the cube root transformation, which is necessary to adequately model value and chroma in the Munsell color system [4].

Following the publication of Romney and Chiao [1] we encountered work on complementary colors by MacAdam [9] published over 70 years ago. In that article MacAdam presented a plot of a curve (his Fig. 3) that, except for scale, is almost indistinguishable from our Fig. 2. He labeled this curve as "Moment of one watt of indicated wavelength" and said that is was derived as "a consequence of the objectively verifiable laws of additive color mixture[9]." The physical measurement was determined by investigating how many watts of complementary spectral light were necessary to

neutralize one watt of indicated wavelength. His research involved complementary spectral colors and posed the question of how much of each was necessary to obtain a neutral white. Since he used 1931 standard observer data rather than the Stockman and Sharpe data that became available more than 50 years later, his peaks and troughs are slightly different from those marked with dashed vertical lines in Fig. 2 (his 448 nm is identical to ours, and the others are 490 nm, 569 nm, and 605 nm).

[Place Fig. 2 about here]

In MacAdam's derivation the short-wavelength peak is complementary to the second wavelength trough and the long-wavelength peak is complementary to the first wavelength trough, as is indicated by the two arrows in our Fig. 2. Fig. 3 is a plot of vectors from the origin to these pairs of complementary spectral lights on the spectral color boundary and they are in close accord with MacAdam's derivation.

The spectral color boundary in Figs. 1 and 3 is a projection of a three-dimensional plot of the three visual system sensitivity curves onto the two-dimensional chromaticity plane of the Munsell conceptual system. The Munsell value dimension is perpendicular to the chromaticity plane and therefore the origin at the center of the figure is an equal energy light of some constant value from 0 (black) to 1 (white). The idea of plotting a figure like this goes back to Adams [10] who noted in 1942 that "any chromaticity diagram is a radial projection, onto a suitably oriented plane, of some three-dimensional tristimulus diagram" [Ref.10, p. 168]. Since the Stockman and Sharpe (3) cone sensitivities are a linear transformation of the Stiles and Burch [5] color matching functions, they constitute a legitimate tristimulus diagram. Adam's presents a stereoscopic view of the "equal-energy" spectrum locus using I. C. I. Standard Illuminant C that, after reflection, is a close analogue of the spectral color boundary in Figs. 1 and 3. Over 35 years ago Thornton [11] derived a spectral color boundary of the same shape based on the number of watts of a complementary spectral color required per watt at a given wavelength to generate daylight chromaticity. The shape of the figure in Thornton's Fig. 9 is a very close analogue of the spectral color boundary in Figs. 1 and 3 while his Fig. 10 is computed in the same way as our Fig. 2 (distance of spectral color boundary from origin) and is very similar in shape.

[Place Fig. 3 about here]

Because the MacAdam paper [9] was not cited by either Adams [10] or Thornton [11] and Burns, Cohen, and Kuznetsov [8] did not cite any of the three, we have four independent confirmations, by different methods, of the proper shape of the spectral color boundary of human chromatic sensitivities that validate the curve derived by Romney and Chiao. The fact that the earlier work relates the spectral color boundary to physical energy units measured in watts is especially noteworthy and important to stress. A final confirmation of the Romney and Chiao model is that it provides a functional explanation for the placement of the MacAdam's complementary pairs of colors in Fig. 3B, namely that they constitute the collapsed color dimensions for two types of dichromate color blindness. Protanopes perceive color only along the dimension from blue to yellow as is indicated by the pair of wavelengths connected by the top arrow in Fig. 2 and the vector in Fig. 3 connecting the blue spectral color at 448 nm with its complement at 566 nm. Tritanopes perceive color only along the dimension from cyan to red as indicated by the pair of wavelengths connected by the bottom arrow in Fig. 2 and the vector in Fig. 3 connecting the red spectral color at 601 nm with its complement at 485 nm. These dichromat dimensions are derived by Romney and Chiao ([1]) and illustrated in their Fig. 3.

A careful study of the three figures shown above reveals an explanation of the so-call purple paradox that has bothered some researchers since the time Newton first decomposed apparently white sunlight into the spectral colors with his prism experiments. The problem can be seen in any CIE chromaticity diagram where colors are represented within a horseshoe shaped curve closed by a line at the bottom called the purple line. The problem arises from the observation that there is a gap in the color circle for spectral (monochromatic) colors but not for surface colors. The reason for this is that surfaces reflect some light at each wavelength so that a normal surface has a spectrum consisting of a mixture of lights reflecting from all wavelengths from 400 nm to 700 nm. Human perceptions of the color of an object are derived from how the three cone photoreceptors are differentially simulated across the visible spectrum from the light reflected from that object. The three curves shown in Fig. 3A represent a very abstract and mathematically derived model for the final coding for color perception. The model predicts that the sensitivity to a monochromatic light at the ends of the spectrum is virtually nil and there is no purple, thus the color circle has a gap if color stimuli are

limited to a single wavelength. The model predicts that the shape of a chromaticity diagram limited to pairs of three primary monochromatic lights would be a triangle. Finally, the model predicts that the shape of a chromaticity diagram consisting of triads of three primary lights at the prime locations shown in Fig. 1 would include the full of gamut of a modern color television set or a color digital camera. The reflectance spectra of natural surfaces are limited in appearance to the visual sensitivities of the observer, illustrated for a normal observer in Figs. 1 to 3.

3. COMPARING REFLECTANCE SPECTRA WITH MUNSELL THEORY

Romney and Chiao measure the adequacy of their model by comparing its predictions with the CIE L*a*b* [4] color system. In this paper we compare the predictions of the model with the Munsell color system. Before projecting the reflectance spectra through the orthonormal cone projection matrix we will smooth the spectra by averaging the chromaticity signal of complementary Munsell chips. MacAdam's research on complementary spectral lights suggests that when complementary reflectance spectra are combined in appropriate proportions, as in a Maxwell color wheel, an achromatic white or gray should be perceived. Ideally complementary reflectance spectra in the Munsell system should have equal chroma values. To partially compensate for deviations from this ideal we propose to take all complete hue circles of 40 chips in the Munsell system that are matched on both value and chroma and smooth the reflectance spectra of complementary pairs by averaging the spectra with their complement. In effect we hope to improve the accuracy of the estimates of the conceptual location of the Munsell chips by averaging the production and other errors made in complementary pairs. To the extent to which errors on opposite side of the color circle are independent of each other an averaging of the location should reduce overall error.

The Munsell reflectance data consist of reflectance spectra measured in percentage reflectance (scaled 0 to 1) at each nm from 400 nm to 700 nm for the 1,269 color samples. These data and their source are described by Kohonen et al. [12]. Among the 1,269 samples there are 16 complete hue circles matched on value and chroma as follows: chroma=2 at values=3 to 8, chroma=4 at values=4 to 8, chroma=6 at values=5 to 7, and chroma=8 at values=6 and 7. Thus our sample consists of a symmetrical subset of 640 sample color chips constituting 16 complete hue circles of 40 chips each.

[Place Fig. 4 about here]

The smoothing procedure is carried out after taking the cube root, element wise at each nm, of each spectrum. Fig. 4 shows a pair of complementary reflectance spectra before and after smoothing. In panel A, the green line represents the Munsell chip 5 Green 7/8 (value=7 and chroma=8) and the magenta line represents Munsell chip 5 Red-Purple 7/8. Representing the raw reflectance spectra as g and m and the smoothed curves as g* and m*, we first compute the mean of each vector and take the overall mean $a = (\bar{g} + \bar{m})/2$ and save the result *a* for later use. The curves $g^+ = g - \bar{g}$ and $m^+ = m - \bar{m}$ remaining after subtracting the means are shown in panel B together with their complements $g^- = -1 \times (g - \bar{g})$ and $m^- = -1 \times (m - \bar{m})$ obtained by reversing the sign at each value. The smoothed curve g* shown in panel C is obtained by averaging the positive *g* curve and the negative *m* curve in panel B and adding back the overall mean. The smoothed curve m* is obtained in a similar way with the positive m curve and negative g curve. In mathematical notation we get $g^* = a + g^+ + m^-$ and $m^* = a + m^+ + g^-$. The smoothed data for all 640 chips are then multiplied by the projection matrix, obtained using the Stockman and Sharpe cone sensitivity curves. The data are then scaled, using singular value decomposition, in Euclidean space.

4. MODELING COLOR WITH AND WITHOUT AN OBSERVER

Earlier we [13] proposed a model for relating reflectance spectra space to the Munsell appearance space without any observer. If we apply Eq. 3 from that article and to the 640 smoothed reflectance spectra, we obtain the results shown in Fig. 5A. The spectral color boundary of the raw reflectance spectra is a horseshoe shape in contrast to the three-lobed shape of the spectral color boundary obtained using the projection matrix based on an observer as in Fig. 5B. The horseshoe shape is somewhat reminiscent of the CIE chromaticity diagram [4].

The results shown in Fig. 5 deserve careful examination. First we need to explain in more detail and clarify exactly what the results are. The effect of the smoothing procedure may be seen clearly by comparing the location of all 1,269 Munsell chips in Fig. 1 with the location of the 640 smoothed Munsell chips in Fig. 5B. Note that the center of gravity of the figure is off center in Fig. 1 and is exactly centered in Fig. 5B. In

addition the overall structure of the Munsell system is much more apparent and the chroma circles are clearly defined.

[Place Fig. 5 about here]

Perhaps the most striking thing about Fig. 5B is the close correspondence of the structures connected by the vectors. The filled dots represent the locations of the chips as seen by a normal observer with Stockman and Sharpe cone sensitivities. The ends of the vectors represent the location of the chips as analyzed purely in terms of the reflectance spectra as physical measurements without any observer involved. As a quantitative measure of the similarity of the two structures we can use the Stewart-Love [14] redundancy index, a measure of the proportion of variance accounted for in one set of variables by another set (a multivariate version of r^2 between two individual variables). The Stewart-Love index between the coordinates with an observer and without an observer is 0.9988. Evidence that this degree of correspondence is not an artifact of the smoothing procedure is found in an article on prime colors [15] that reports a Stewart-Love index of 0.9983 between a Euclidean model of the 1,269 Munsell chips without an observer and an earlier model involving an observer from D'Andrade and Romney [16]. Romney and Fulton [15] noted, "Of interest is the fact that the Euclidean model of the cube root of the reflectance spectra provides virtually identical information as the models based on psychophysically derived color matching functions[15, p. 15702]."

Another striking fact is the close fit to the conceptual Munsell system. The Steward-Love index between the Munsell conceptual coordinates and those of the model coordinates with or without an observer is 0.995. This fit is affected by the smoothing procedure as indicated by a previously reported [15] Stewart-Love index or 0.977 between the Munsell conceptual coordinates and the cube-rooted Euclidean model. In our opinion the original Munsell chips have systematic departures from their aiming points as described in an earlier article [13]. Still, the Munsell system has many features that recommend its use, one of which is the complete symmetry of complements that correspond to afterimages [1], another is the mixing of complements to produce achromatic colors as in Maxwell color wheel-mixing [9]. Thus each hue spoke in the Munsell structure and its complement plot on a line that passes through the origin. Equally important is the equal perceptual spacing of the hue spokes of the system. It is

clear that a much improved atlas could be produced that would correspond exactly with the conceptual Munsell structure [13,17].

The most useful feature of the model and the results displayed in Fig. 5B is the fact that the set of all possible reflectance spectra after multiplication by the projection matrix constitute a vector space that may defined as $\mathbf{X}$ and $\mathbf{x}_i \in \mathbf{X}$. Within this set any combination [18] of elements from $\mathbf{X}$ follows the rules of convex combination and is defined as a linear combination of the form

$$\alpha_1\mathbf{x}_1 + \alpha_2\mathbf{x}_2 + \cdots + \alpha_n\mathbf{x}_n, \qquad (1)$$

Where $\mathbf{x}_i \in \mathbf{X}$, each $\alpha_i \leq 0$, and the α_i sum to 1. It follows that distances in the space are invariant with respect to orientation. An example of the use of convex combination in a color space without an observer is given in Romney [13]. This means that a uniform color space is possible in both theory and practice and that the MacAdam error ellipses would plot as circles in this space [19,9,4].

To illustrate the possibility of a uniform color space, we might examine the way a sample taken from the Optical Society of America Uniform Color Scales (OSA-UCS)[20] would appear in the Munsell space shown in Fig. 5B. The OSA-UCS chips were designed as a uniform color system [21,22,23]. The theoretical locations of the samples are embedded in a three dimensional Euclidean space with a cuboctahedral shell with 12 points at unit distance from a central point of origin. The dimensions are, L, which represents lightness where L=0 represents a neutral gray close to Munsell Value 6 with lighter shades positive and darker negative; j, which represents a yellow-blue dimension with yellow on the positive side;, and g which represents a pink-green dimension with green on the positive side. We measured the reflectance spectra (Ocean Optics spectrometer USB2000) of 49 chips in the L=0 plane and appended them to the 640 smoothed Munsell spectra and then used the model to obtain the results shown in Fig. 6. We might note that this method could be used to find chips in the Munsell system that match chips in the OSA-UCS system rather than depending on subjects matching chips was done by Boynton et al. [24]. Deviations from the ideal theoretical locations are caused by errors in the production of the chips and measurement errors on our part. The orientation of the OSA-UCS is different that our plot of the Munsell system. The correct axes of the OSA-UCS system are shown by the diagonal lines in Fig. 6.

[Place Fig. 6 about here]

5. SPECTRAL LIGHTS VERSUS NARROW AND BROAD BAND SPECTRA

Color vision evolved to distinguish among spectra arriving at the retina from various objects in the visual field. In large part these were reflectance spectra from objects such as leaves, fruit, and animals, etc. Spectra from other objects such as the blue sky arise as a result of Rayleigh scattering, which can be computed from theory or measured in practical terms. In any event the objects that were relevant for evolution had broad band smooth spectra regardless of how they were produced. Nassau [25] and Tilley [26] describe in detail the many physical and chemical processes that give rise to the spectra of objects. Since reflectance spectra of ordinary surfaces are common and easily available, they are frequently used as we the use reflectance spectra of Munsell color chips. The present model, however, should predict the appearance of any spectrum in the range of 400 nm to 700 nm that arrives at the retina.

In contrast to broad band smooth spectra, much of color vision science is based on color matching functions [4] derived from very narrow band spectral lights. Since it was not designed to represent color appearance, the spectral locus in the CIE chromaticity diagram [4] is a severe distortion of human perception of spectral colors since it shows the locus as horseshoe-shaped rather than correctly as in Fig.5B. Color is derived from human perceptions determined by a combination of the cone sensitivity curves and the way the brain (of which the neurons in the retina are part) computes the differential stimulation of the different classes of cone receptors by the spectra arriving at the retina. The appearance of extremely narrow-band spectral light is represented by its location in the spectral color boundary. A normal surface reflects some light at each wavelength and its appearance is computed from a weighted combination of all wavelengths in which the weights are a function of the sensitivity curve shown in Fig. 2. All other spectra, artificial or natural, that arrive at the retina are computed in a similar way. The current model provides a way to estimate the results of that computation. It makes no claim to resemble the way the biological organism makes the calculations. It does not resemble the actual neural implementation of color vision any more electronic computation resembles the way a human performs addition. It does, however, provide that correspond to the answers arrived at by any human observers (given their cone sensitivity functions).

As a preliminary check on the model, we can plot some familiar theoretically derived curves; some Planck [4] blackbody radiation temperature curves in the visible range, the Rayleigh [26] curve, based on the scattering by gas molecules in the atmosphere that gives rise to the blue appearance of the sky, and some flat curves of constant value to represent flat light as assumed in the model. To estimate their location in Munsell space we append the artificial spectra to the Munsell color chip spectra and run the whole set through the model including the cube-rooting procedure. The results are shown in Figure 7.

[Place Fig. 7 about here]

The Planck curves form an arc with a slight curvature. If the two end points were connected with a line it would pass through the center of the diagram on the 5 Yellow vs. 5 Purple-Blue axes. The arrow at the left in Fig. 7B points to the location of the Rayleigh theoretical scattering curve appearance as predicted by the model. The closest Munsell color chip, just below and to the right, is Munsell 5 Purple-Blue value=7 and chroma=8, an ideal match for sky blue in our judgment. The arrow at the right in Fig. 7B points to the location of the predicted appearance of a Planck blackbody radiation of 4,000 K. The closest Munsell color chip, just below and to the left, is Munsell 5 Yellow value=7 and chroma=4.

The interval between the location of 4,000 K and 3900 K is of special interest since MacAdam [27] used it as one of the locations in his study of error ellipses established around 35 standard chromaticities. The boundaries of these error ellipses were determined from the results of over 20,000 separate color matches by a single young observer, PGN, who had normal color vision. MacAdam found that "a difference of 100 K of color temperature near 4,000 K is slightly more than twice the standard deviation of chromaticity matching by PGN. Therefore, it is just noticeable and slightly more than half as noticeable as the difference between the sodium D lines [another of his standard chromaticities]" [19, p. 136]. The diameters of the chroma=8 circles in the Munsell color samples as shown in Fig. 7B are 50 times this color appearance difference. Since we have a restricted sample of chroma values a more realistic range would be closer to chroma=16 giving a diameter of 100 rather than 50. The cube of 100 is a million, an extremely crude estimate for the number of distinguishable colors.

A final example shows how the model may be used to obtain predictions for the appearance of synthetic spectra that are theoretically relevant and could serve to confirm or disconfirm the model. It was directly stimulated by the imaginative research of Mizokami et al. [28] on nonlinearities in color coding and the Abney effect. In particular they looked at the effects of differential changes in hue of narrow (25 nm) and broad (105 nm) band lights as a function of wavelength (see their Fig. 4). The Romney and Chiao model provides both a functional explanation of their results and a way to calculate the appearance of narrow and broad band spectra at different wavelengths. The four wavelengths shown in Figs. 2 are a natural choice for a simple and critical test of the model. Since sensitivity at the ends of the wavelength range declines to zero, it seems reasonable to expect that the effect of a change of band width there will have a bigger effect there than in the middle wavelengths. To understand how increasing band width might change hue, focus on the short wavelength sensitivity peak in Fig. 2 marked with the vertical dotted line representing the location of a monochromatic spectral light. If we imagine expanding the band width of the light equally to both sides, we see that at some point the center of gravity of the weighted average of overall sensitivity has to move to a longer wavelength because the sensitivity curve goes to zero on the short wavelength end. The same argument holds for the location marked at 601 nm where the gravity has to shift to a shorter wavelength because the long side goes to zero. For the two points marked at 485 nm and 566 nm, in contrast, any expansion of the band width increases more or less evenly within fairly wide bounds.

The test consists in taking these four critical wavelength locations and making a strong prediction that a modest increase in bandwidth will have little or no effect at 484 nm and 566 nm and will change hue to a longer- wavelength appearance at 448 nm and to a shorter wavelength-appearance at 601 nm. To simulate the spectra we choose Gaussian curves with means at the above mentioned locations and standard deviations for the narrow band width of 20 nm (half height width=48 nm) and 40 nm (half height width =94 nm)for the broad band width. In order to keep the chroma values in reasonable correspondence with the natural range of the Munsell spectra, we added a constant of 0.2, a number determined with a few trial-and-error iterations. This does not alter the quality of the results significantly. These simulated spectra are shown in Fig. 8A. As in the

previous example of artificial spectra, these eight spectra were appended to the smoothed Munsell color chip spectra and the combined set was analyzed using the model. The results are shown in Fig. 8B.

[Place Fig. 8 about here]

The results are basically as predicted. Small deviations of the simulated Gaussian curves from monochromatic spectral colors in Fig. 3 may be the result of adding a constant. Change in the appearance of the narrow versus broad band at the short and long wavelength location were in the predicted direction and amounted to about three Munsell hue categories, a rather large perceptual difference. This simple, rather mechanical, functional explanation provided by the model takes all the mystery out of the effect that bandwidth has on hue.

Substantial confirmation of the predictions of the model is provided in recent work by Crognale et al. [29] who were able to artificially create spectra of any band width with peaks located at any location. They used a narrow bandwidth curve of 25 nm (half height width) and a wide bandwidth curve of 80 nm (half height width) to investigate the effect of differences in bandwidth on appearance. The wide bandwidth curve was taken as a target reference at peak wavelengths from 450 nm to 650 nm in 20 nm intervals. The task was to match the hue of the target appearance with the narrow band appearance by moving the peak of the narrow band up or down the nm scale using an interleaved staircase design. Results were reported as the difference in nm between the peak location of the matching light and the peak location of the target reference light in their Fig. 3. The results correspond with our results as closely as can be visually determined from an examination of their plot. The direction of the deviations we found for the long and the short wavelengths correspond to their findings and our finding of no change at about 485 nm and 566 nm corresponds closely with zero crossing points in their plot. Our analysis was done before we were aware of their work. Despite the different bandwidths used, the close correspondence of our model predictions and the results of the empirical findings of Crognale et al.'s is remarkable. The advantage of our model is that the results were derived in advance from the application of the model that provides a functional explanation of the results.

9. SUMMARY

A previously reported functional model of color coding proposing a spectral color boundary very different from the one normally portrayed in CIE chromaticity diagrams has been shown to be strongly supported by research done many decades ago. Using the model to predict the appearance of selected Munsell color chips to a normal human observer produces results virtually identical those obtained by analyzing the chips without taking any observer into account. It appears that humans perceive the color appearance of most ordinary objects, such as Munsell color samples, primarily on the basis of the reflectance spectra of the object. The color appearance of objects or things whose spectra are generated by processes other than reflectance, such as the sky, are based on the spectra arriving at the retina from the object. The model predicts color appearance from the photoreceptor sensitivity curves of the observer and the spectra coming from the object. Analysis of various theoretical and synthesized spectra, including Planck black body temperature curves, the Rayleigh scattering curve for sky blue, curves of constant value representing achromatic colors, and various narrow and broad band artificial spectra synthesized to model aspects of the Abney effect, has demonstrated that the model applies to any spectra reaching the retina, regardless of bandwidth.

The Munsell color system has several characteristics that make it optimal for the description and understanding of color appearance. First, a color arising from reflectance spectra has a complement that lies on a line passing through the origin of the color space. (Although not all monochromatic spectral lights have monochromatic spectral complements, complements may be formed by some mixture of spectral lights.) Second, complements predict the perceived color of afterimages. Third, the color circle is perceptually continuous with no gaps and the equal angles between the spokes in the Munsell system represent uniform hue transitions at a given chroma value.

We have shown how various theoretical curves such as Planck black body temperature function, Rayleigh scattering curves for sky blue, and lines of constant values may be represented in Munsell space. We also shown that the model to provides straight forward functional predictions for modeling the effects of differing band widths on the perception of hue at differing wavelengths. Further explorations using the model can be expected to yield further fruitful applications.

References

1. A. K. Romney and C.-C. Chiao, "Functional computational model for optimal color coding," Proceedings of the National Academy of Sciences **106**(25), 10376–10381 (2009).
2. I. Munsell Color Company, *Munsell Book of Color: Matte Finish Collection* (Munsell, 1976).
3. A. Stockman and L. T. Sharpe, "The spectral sensitivities of the middle- and long-wavelength-sensitive cones derived from measurements in observers of known genotype," Vision Research **40**(13), 1711–1737 (2000).
4. G. Wyszecki and W. S. Stiles, *Color Science: Concepts and Methods, Quantitative Data and Formulae,* 2nd ed. (John Wiley & Sons, New York, 1982).
5. W. S. Stiles and J. M. Burch, "N.P.L. Colour-matching Investigation: Final Report (1958)," Journal of Modern Optics **6**, 1–26 (1959).
6. J. B. Cohen, *Visual Color and Color Mixture: The Fundamental Color Space* (University of Illinois, Urbana, 2001).
7. J. B. Cohen and W. E. Kappauf, "Metameric color stimuli, fundamental metamers, and Wyszecki's metameric blacks," The American Journal of Psychology **95**(4), 537–564 (1982).
8. S. A. Burns, J. B. Cohen, and E. N. Kuznetsov, "The Munsell-color system in fundamental color space," Color Research and Application **15**(1), 29–51 (1990).
9. D. L. Macadam, "Photometric Relationships Between Complementary Colors," J. Opt. Soc. Am. **28**(4), 103–103 (1938).
10. E. Q. Adams, "X-Z Planes in the 1931 I.C.I. System of Colorimetry," Journal of Optical Society of American **32**, 168–173 (1942).
11. W. A. Thornton, "Luminosity and Color-Rendering Capability of White Light," J. Opt. Soc. Am. **61**(9), 1155–1163 (1971).
12. O. Kohonen, Jussi Parkkinen, and Timo Jääskeläinen, "Databases for spectral color science," Color Research & Application **31**(5), 381–390 (2006).

13. A. K. Romney, "Relating reflectance spectra space to Munsell color appearance space," J. Opt. Soc. Am. A-optics Image Science and Vision **25**(3), 658–666 (2008).
14. D. Stewart and W. Love, "A general canonical correlation index," Psychological Bulletin **70**, 160–163 (1968).
15. A. K. Romney and J. T. Fulton, "Transforming reflectance spectra into Munsell color space by using prime colors," Proceedings of the National Academy of Sciences of the United States of America **103**(42), 15698–15703 (2006).
16. R. G. D'Andrade and A. K. Romney "A quantitative model for transforming reflectance spectra into the Munsell color space using cone sensitivity functions and opponent process weights," Proceedings of the National Academy of Sciences of the United States of America **100**(10), 6281–6286 (2003).
17. J. J. Koenderink, "Color atlas theory," J. Opt. Soc. Am. A **4**(7), 1314–1321 (1987).
18. G. Strang, *Linear Algebra and Its Applications*, 3rd ed. (Harcourt, Brace, Jovanovich, San Diego, CA, 1988).
19. D. L. Macadam, *Color Measurement: Theme and Variations*, Springer Series in Optical Sciences (Springer-Verlag Berlin Heidelberg New York, 1981).
20. O. S. o. America, *Uniform Color Scales* (Crowell, New York, 1974).
21. D. L. MacAdam, "Uniform color scales," J. Opt. Soc. Am. **64**(12), 1691–1702 (1974).
22. D. Nickerson, "OSA uniform color scale camples-A unique set," Color Research and Application **6**(1), 7–33 (1981).
23. F. W. Billmeyer, "On the geometry of the OSA uniform color scales committee space," Color Research and Application **6**(1), 34–37 (1981).
24. R. M. Boynton, R. E. Maclaury, and K. Uchikawa, "Centroids of color categories compared by 2 methods," Color Research and Application **14**(1), 6–15 (1989).
25. K. Nassau, *The Physics and Chemistry of Color: The Fifteen Causes of Color*, 2nd ed., Wiley Series in Pure and Applied Optics (John Wiley & Sons, Inc., 2001).

26. R. Tilley, *Colour and the Optical Properties of Materials* (John Wiley & Sons, Inc., 2000).
27. D. L. Macadam, "Visual Sensitivities to Color Differences in Daylight," J. Opt. Soc. Am. **32**(5), 247–273 (1942).
28. Y. Mizokami, J. S. Werner, M. A. Crognale, and M. A. Webster, "Nonlinearities in color coding: Compensating color appearance for the eye's spectral sensitivity," Journal of Vision **6**(9), 996–1007 (2006).
29. M. A. Crognale, M. A. Webster, and A. Y. Fong, "Application of digital micromirror devices to vision science: shaping the spectrum of stimuli," Proceedings of SPIE **7210**, 1–7 (2009).

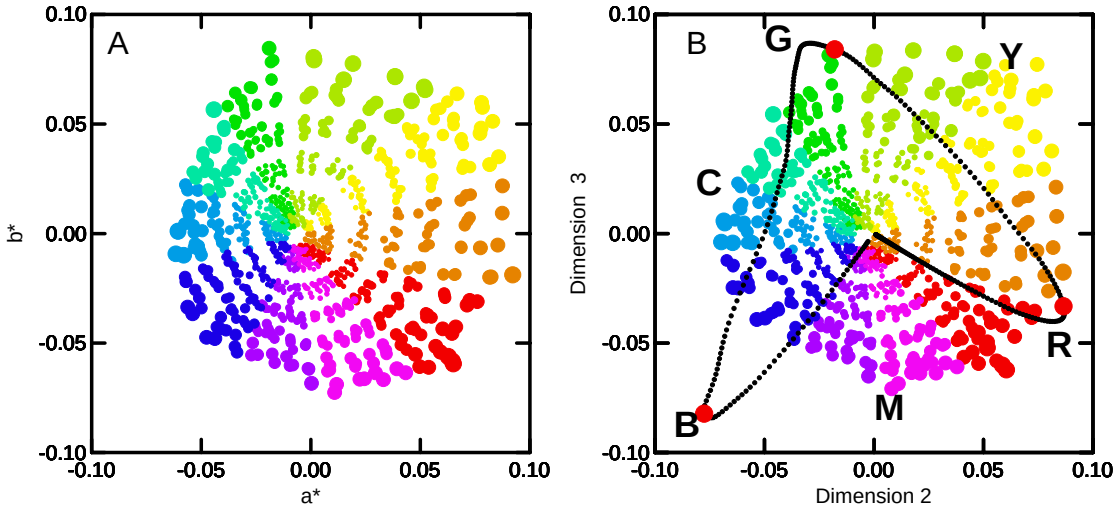

Fig. 1. Comparison between CIE L*a*b* color system and estimates of the model. (A) CIE L*a*b* color locations of the Munsell chips rotated to the orientation of the model output to facilitate comparison. (B) Model output results for dimensions 2 and 3 of 1,269 Munsell chip locations and for 301 wavelength locations. The first achromatic dimension is perpendicular to these two dimensions and is not shown here. Colors represent hue segments and are otherwise arbitrary. The spectral color boundary locations for each nm appear in black with prime color wavelengths highlighted with large red dots. The large bold letters represent the additive primaries of red, green and blue and the subtractive primaries of yellow, magenta, and cyan.

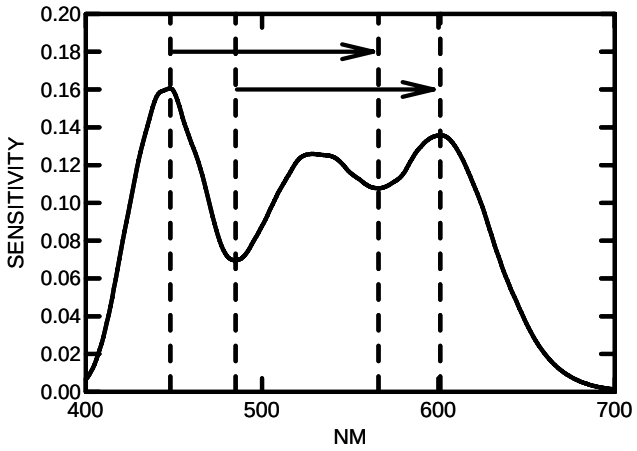

Fig. 2. Normal human visual sensitivities computed from the Euclidean distance of the spectral color boundary from the origin. The four dotted lines indicating peaks or troughs appear at 448 nm, 485 nm, 566 nm, and 601 nm. The top arrow connects the blue spectral light at 448 nm with its complementary yellow spectral light at 566 nm while the lower arrow connects the cyan spectral light at 485 nm with it complementary red spectral light at 601 nm. The three peaks correspond to the three lobes in Fig. 1.

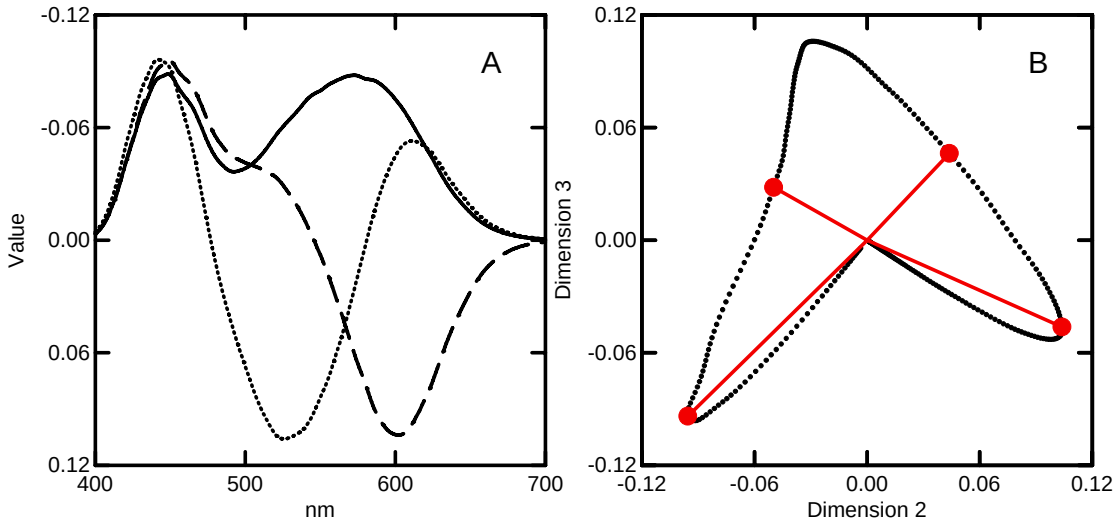

Fig. 3. Coordinates of spectral light curves. (3A) Wavelength light coordinates plotted against nm (solid line=first dimension, dashed line=second dimension, dotted line=third dimension). (3B) A plot of the second and third dimension coordinates that constitute the spectral color boundary with red vectors connecting the origin with MacAdam's complementary pairs of wavelengths. The short-wavelength blue sensitivity lobe is in the lower left side and the long-wavelength red sensitivity lobe is on the right side of the plot.

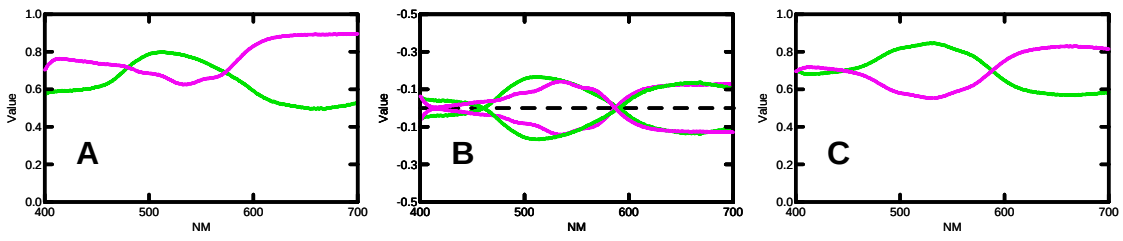

Fig. 4. Various stages of the smoothing process for a pair of complementary Munsell color chips, namely 5 Green 7/8 and 5 Red-Purple 7/8. (A) The cube-rooted reflectance spectra. (B) The reflectance spectra and their complements after subtracting the mean from each reflectance spectrum. (C) The smoothed reflectance spectra after averaging each curve with its complement and adding in the mean of the curves in A.

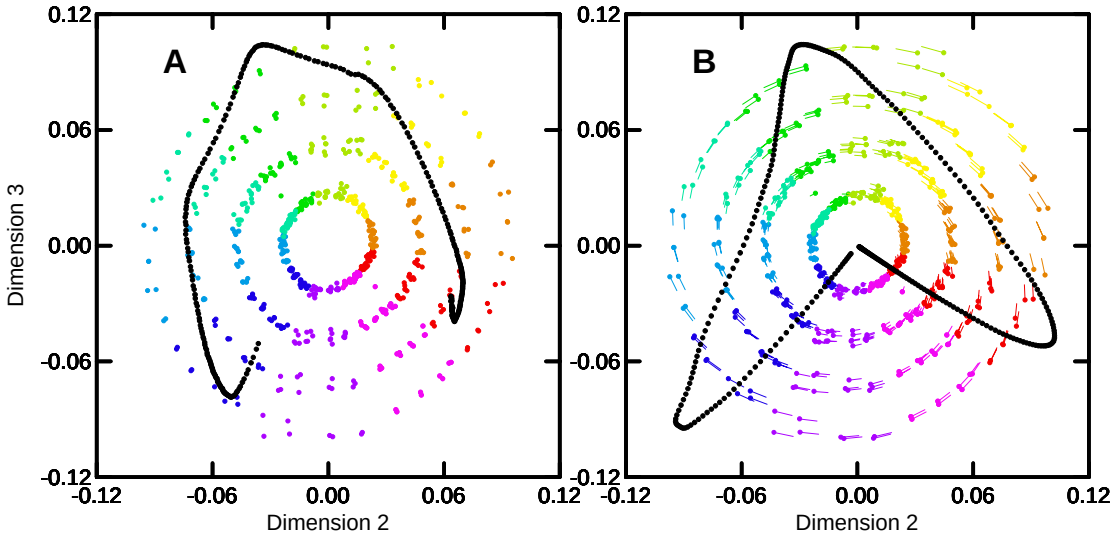

Fig. 5. The relative locations of the smoothed reflectance spectra of 640 Munsell color chips. The colors represent Munsell hue sectors and are otherwise arbitrary. (A) Locations based on smoothed reflectance spectra without an observer. (B) Filled dot locations based on smoothed reflectance spectra after multiplication by a projection matrix based on a normal observer. The ends of the vectors represent the chip locations obtained from the smoothed reflectance spectra without an observer.

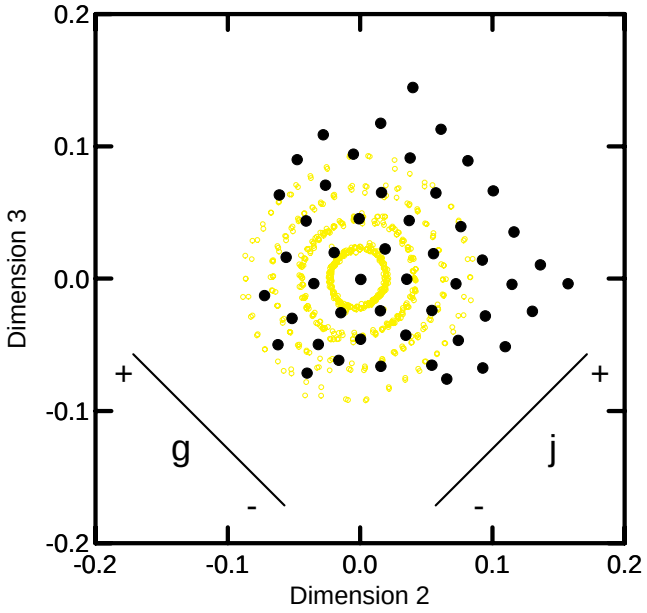

Fig. 6. The results of applying the model to 49 chips in the L=0 plane of the OSA-UCS compared with the Munsell chips located as plotted in Fig. 1. The orientations of the j and g OSA dimensions are indicated by the diagonal lines in the lower corners of the plot. The chips are all even-numbered integers with the neutral gray at the center of the plot.

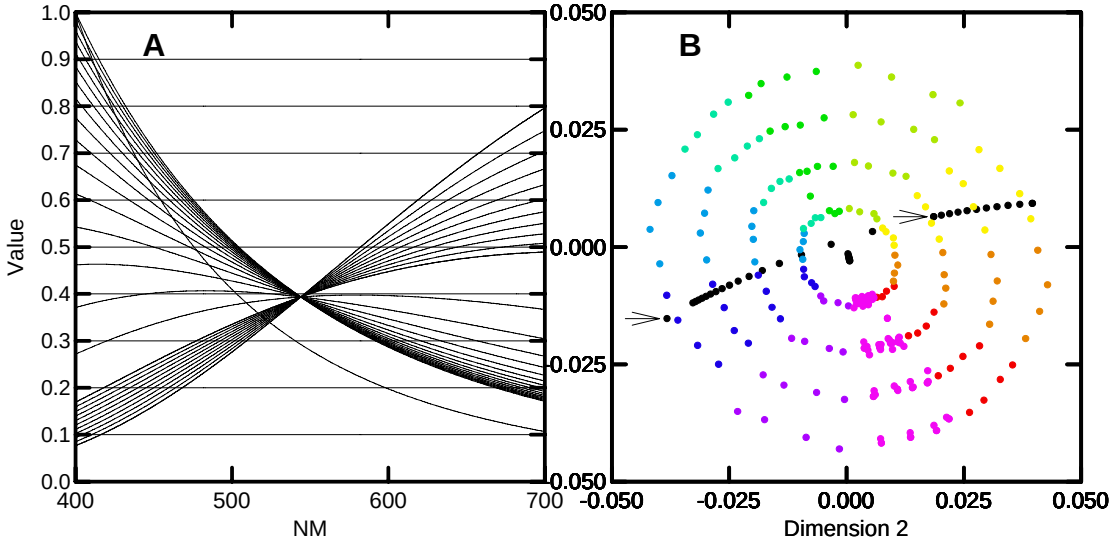

Fig. 7. Examples of spectra computed from theory and their predicted appearance in Munsell color space compared with value=7 smoothed reflectance spectra. (**A**) Theoretical Planck blackbody temperature curves from 3,000 K (top right) to 4,000 K in 100 K steps and from 5,000 K to 20,000 K (bottom right) in 1,000 K steps, theoretical Rayleigh curve (lowest right) for scattering effects giving appearance of blue sky, and nine flat lines of constant value from 0.1 to 0.9. (**B**) Modeled appearance of spectra show in Fig. 6**A** compared with location of Munsell color chips of value=7 (about the average value of the theory-derived spectra). The flat constant lines cluster in the center while the Planck temperature curves form an arc from right (3,000 K) to left (20,000 K). The left arrow points to the Rayleigh curve that lies beyond the Planck arc to the left. The right arrow points to the Planck 4,000 K temperature location.

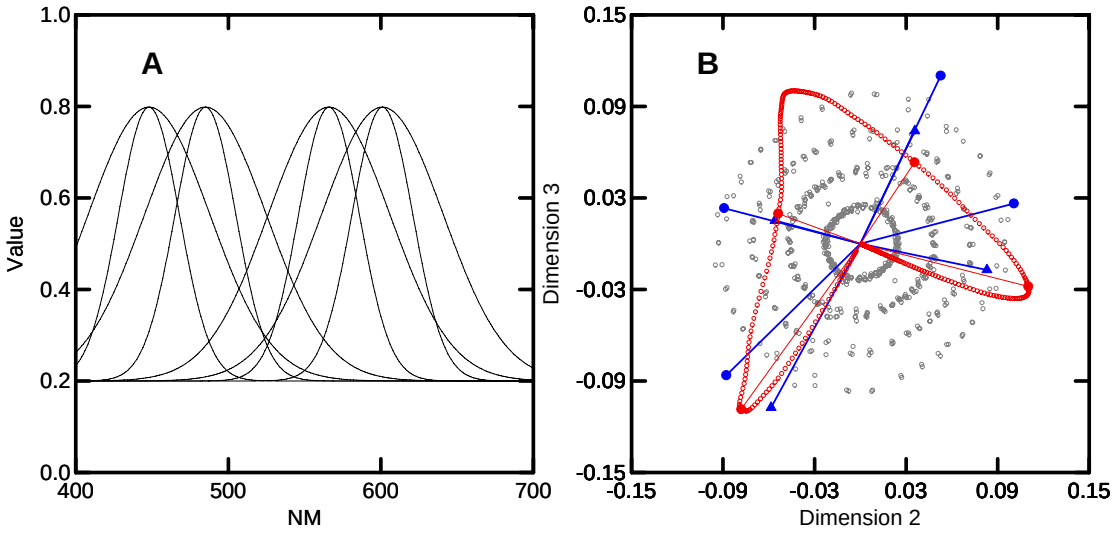

Fig. 8. A plot of four pairs of narrow and broad band simulated spectra and their predicted appearance compared with Munsell color chip spectra. (A) Gaussian curves with peaks at 448 nm, 485 nm, 566 nm, and 601 nm and standard deviation of 20 nm or 40 nm with an added constant of 0.2. (B) Predicted locations of the color appearance of the curves shown in A compared with the appearance of the Munsell color chip spectra. The triangles are narrow band while the circles are broad band. Fig. 3 is superimposed on the results for comparison.